Article

Effective Analytical Techniques for the Condition Monitoring of Induction Motors

Yike Zhang and Barmak Honarvar Shakibaei Asli *

Centre for Life-cycle Engineering and Management, School of Aerospace, Transport and Manufacturing, Cranfield University, Cranfield MK43 0AL, UK

*Correspondence: barmak@cranfield.ac.uk

Abstract: As industrialisation progresses, electric motors are increasingly utilised in manufacturing sectors, and their regular operation plays a crucial role in enhancing production efficiency, safety, and ease. Consequently, there's a growing emphasis on developing technology for monitoring the condition of electric motors. This study focuses on the analysis of common issues like rotor bar failure and eccentricity in induction motors, examining their causes, creating motor models in both normal and malfunctioning conditions through computer simulations, identifying the stator current signals, and comparing their spectra to validate the stator current data. Additionally, this research offers a dependable and efficient dataset for further analysis. The complex and fluctuating nature of the current signals in induction motors necessitates the use of advanced techniques like the tunable-Q wavelet transform (TQWT) and box dimension method for feature extraction, which is more effective in signal characterisation than other approaches. The study then explores the application of Support Vector Machines (SVM) and Artificial Neural Networks (ANN) in fault diagnosis, achieving accuracies of 91.67% and 100%, respectively. The findings indicate that ANN is superior to SVM and suggest this strategy for the automatic detection of motor faults. Implementing such intelligent systems can prevent unexpected and unplanned production interruptions caused by electric motor failures.

Keywords: condition monitoring; induction motors; finite element analysis; wavelet transform; Artificial Neural Network; Support Vector Machine

1. Introduction

Electric machines are utilised in a vast array of industrial applications, ranging from those in power generation, manufacturing, and electric vehicles, to hand tools, household appliances, etc. Of all types of electric motors, induction motors are a common example due to their simplicity of construction, robustness and high efficiency [1]. Electric machine faults could be categorized into internal and external faults, which are further divided into mechanical, electrical and environmental faults. Based on its location in the equipment, faults also could be categorized into the bearing, stator, rotor and other parts of the machine [2]. The electric machine is reliable in operation, but it can suffer from different types of undesirable faults that can lead to unexpected machine breakdowns. Figure 1 displays the statistical analyses of induction motor failure conducted by the Electric Power Research Institute (EPRI), ASEA Brown Boveri (ABB), and the Institution of Electrical and Electronics Engineers (IEEE). According to IEEE and EPRI, the percentage of bearing faults that occur in induction motors during operation is 41% and 42%,

respectively, as seen in Figure 1b,c. Although the probability of meeting a rotor failure is small, the damage to the motor is really huge [3].
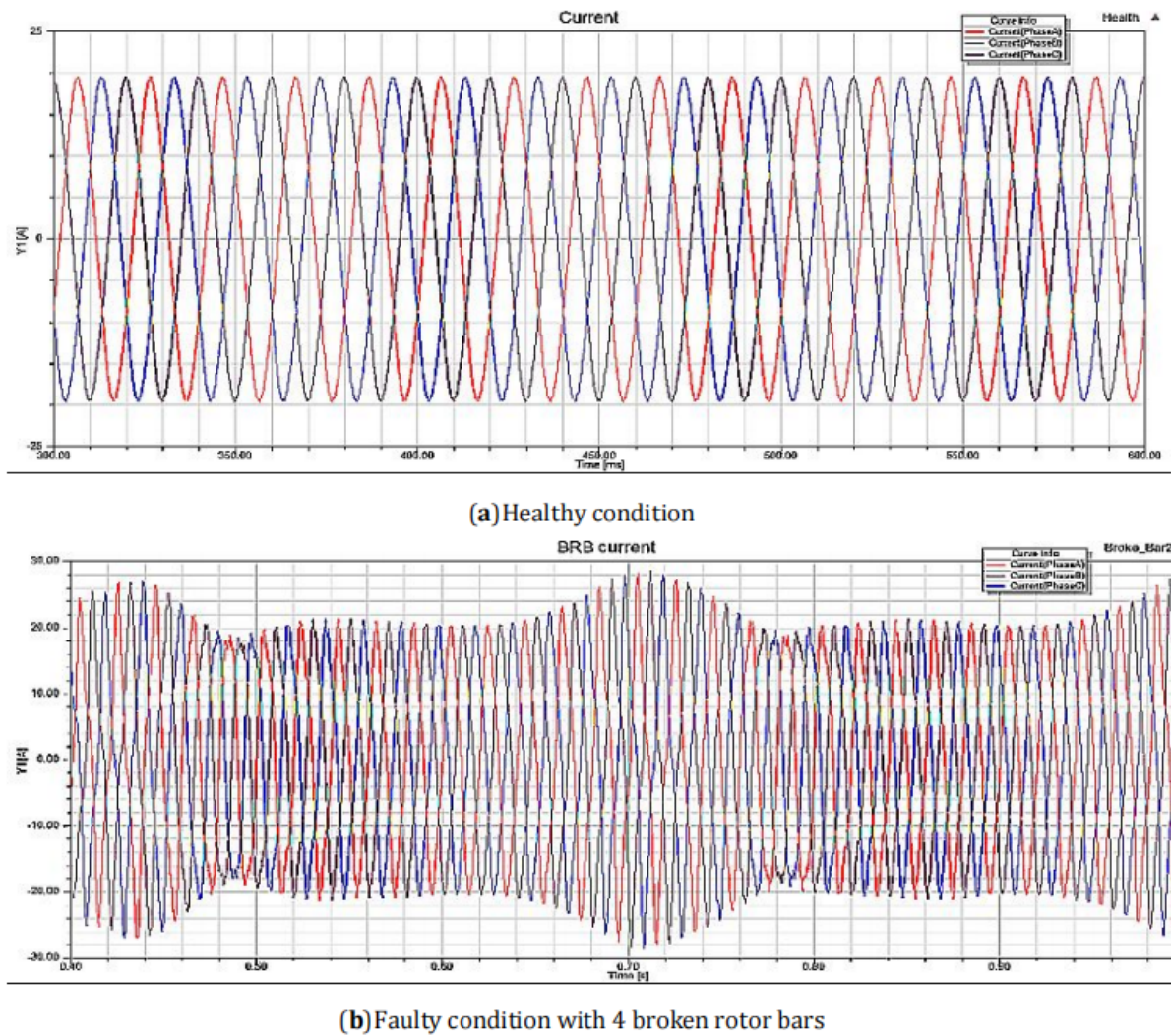

(a) Healthy condition

(b) Faulty condition with 4 broken rotor bars

Figure 1. Study on induction motor faults: (**a**) ABB, (**b**) IEEE, and (**c**) EPRI [4].

It is often vital to ensure a machine is operating robustly and reliably to deliver its intended role and underpin the execution of the wider process it facilitates. Various components of an electric machine can fail, and for a variety of reasons, it is, therefore, beneficial to monitor their operation to help minimise downtime and also maximise lifespan. The combination of fault diagnosis and condition monitoring makes it possible to change the maintenance of electric machines from after-the-fact maintenance to anticipatory maintenance and to avoid the occurrence of malicious accidents with electric machines. Electric machine fault diagnosis is based on the monitoring and detection of motor fault signals, using various methods to analyse the fault signals and the characteristic signals to determine the type of fault [5].

Motor current signature analysis (MCSA) is considered to be one of the most popular diagnostic techniques for monitoring common faults in rotating electric machines [6, 7]. It can detect stator winding faults, bearing faults, broken rotor bars, misalignment and other issues. The MCSA uses the current and voltage signals obtained in the stator to enable monitoring. The current and voltage signals are further processed to produce their power spectrum to determine the cause of the electric machine's fault [8]. Figure 2 shows the general procedure for the MCSA technique. Motor current signals can be obtained from the outputs of current transducers which are placed

non-intrusively on one of the power leads. The resulting raw current signals are acquired by computers after they go through conditioning circuits and data interfaces.
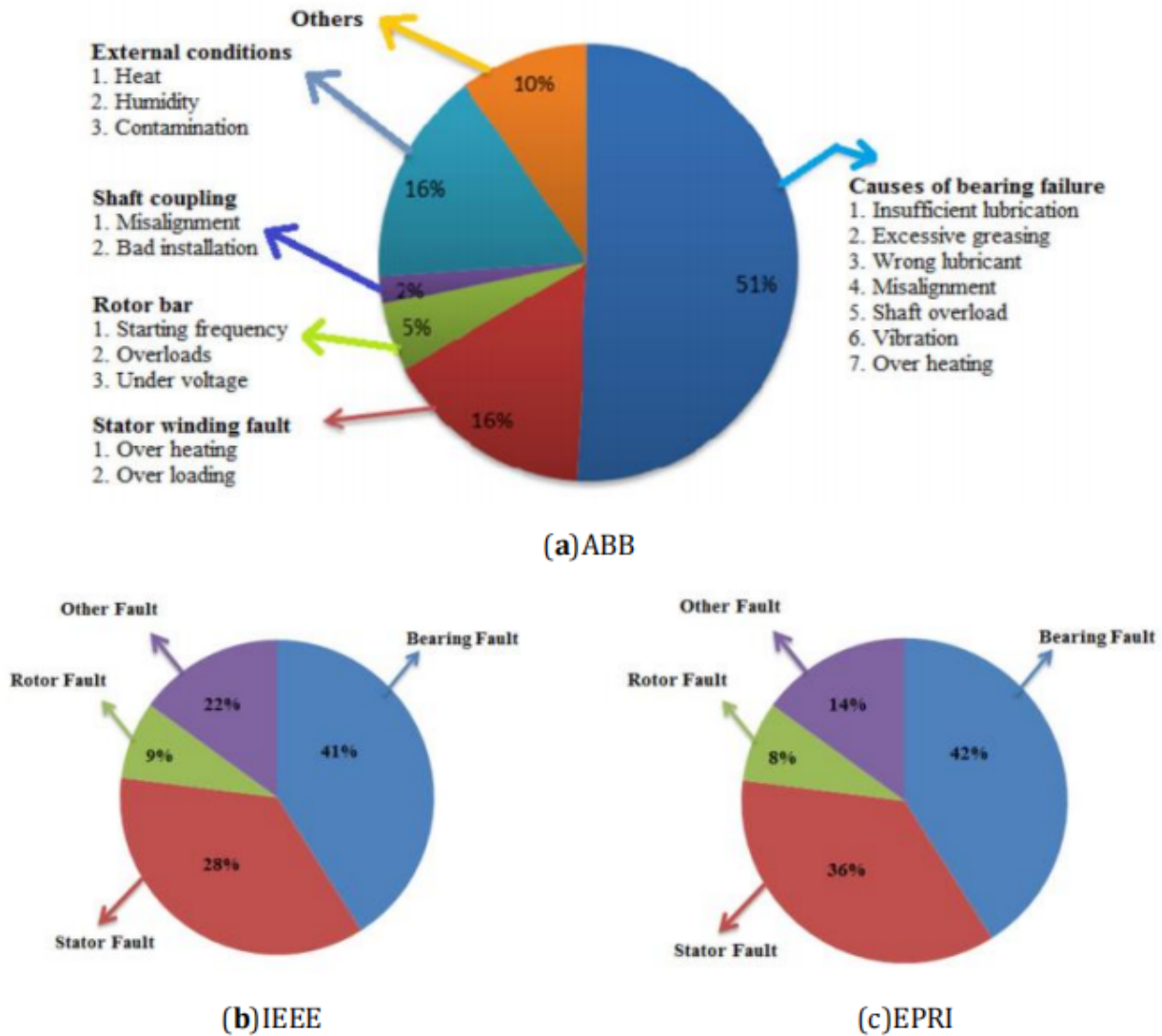

Figure 2. General procedure for MCSA.

As the amount of data is increasing worldwide and computer science is rapidly developing, it is reasonable to remake production using advanced approaches using artificial intelligence (AI) [9]. The AI-based diagnostic system consists of signal-based methods and classification tools such as the Neural Network (NN), Support Vector Machine (SVM) and others [10].

ANNs have been shown to be highly effective in monitoring conditions and forecasting reliability issues due to their flexibility, non-linear behaviour, and their capability to approximate complex functions [11]. This approach is designed to examine and simulate the progression of damage and forecast additional failures based on gathered information [12]. The primary functions of artificial neural networks include classification, prediction, and identification. The concept of artificial neural networks stems from the goal of emulating the learning and error correction capabilities of natural nervous systems by replicating the architecture of the brain's lower levels. Another popular toolset for condition monitoring in machine learning is the support vector machine (SVM). This collection of supervised models is utilized for tasks such as regression, identifying new patterns, reducing the number of features, and SVM, which is particularly effective for classification tasks [13]. SVM is an excellent choice when there is lim-

ited prior knowledge about the data. This method is favoured due to its minimal computational requirements for achieving high levels of accuracy [14].

This paper is organised as follows. Section 2 presents the research methodology for three-phase induction motor condition monitoring. The simulation results of the induction motor, feature extraction and feature classification are discussed in Section 3. This paper's primary contribution is the creation of a simulation model for electrical motor faults. This section also covers the verification of the precision of the TQWT, SWM, and ANN techniques for defect diagnosis. Concluding remarks are discussed in Section 6.

2. Research Methodology

The data preprocessing ensures that the raw signals are adequately prepared for feature extraction and fault diagnosis. By addressing noise, normalization, segmentation, feature enhancement, outlier removal, and baseline correction, it is possible to improve the quality and reliability of the extracted features, leading to more accurate and effective fault diagnosis.

As seen in Figure 3, the signal and data processing are divided into four sections. To get simulation results of current signals, a Maxwell 2D three-phase induction model is developed under health, broken bar fault, and eccentricity fault situations in the first section. Second, in order to have enough data sets accessible to effectively diagnose the issues, data were gathered for testing and training. The wavelet transform was employed in the feature extraction process from the obtained signals, which is described in the third section. Finally, the use of two distinct classifiers, ANN and SVM, for classification and performance evaluation has been covered.
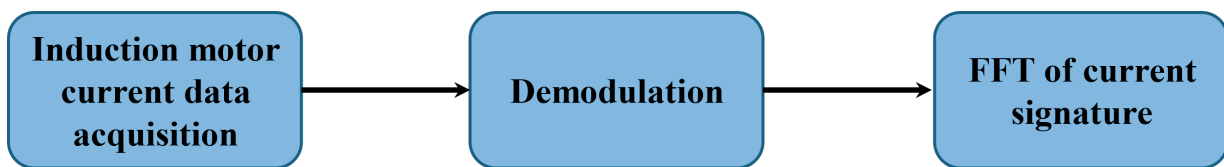

Figure 3. Methodology for three-phase induction motor condition monitoring.

2.1. Simulation of Faults

Taking the common induction motor faults of broken rotor bars and eccentricity faults as examples, the fault mechanism is analysed, the motor model under health and fault conditions is established by Ansys Maxwell software, the corresponding stator current signals are extracted, and the correctness of the extracted stator current data is verified by analysing and comparing the theoretical current spectrum on the one hand; on the other hand, reliable and effective data support is provided for the subsequent feature extraction methods.

Maxwell offers several methods for building finite element 2D models of induction motors, the most convenient of which is to build an RMxprt induction motor model and set the relevant parameters, such as the rated parameters of the induction motor, the stator and rotor settings, etc., then automatically convert it to a Maxwell 2D finite element model using the simulation software [15]. In this paper, an induction motor type Y160M-4 is used as the subject of the study and the relevant parameter values for this type of motor are given in Table 1.

Table 1. Rated parameters of Y160M-6 motor.

Parameter Name	Reference Value	Parameter Name	Reference Value
Rated power	7.5 kW	The inner diameter of the stator	170 mm
Rated current	17 A	The inner diameter of the rotor	60 mm
Rated voltage	380 V	Number of stator slots	36
Rated frequency	50 Hz	Number of rotor slots	26
Rated rotation speed	1500 r/min	Polar number	4

2.1.1. Analysis of Broken Rotor Bar Failure Mechanism

The change in the air gap magnetic field caused by the occurrence of a motor fault is complex and non-linear. When a broken rotor bar fault occurs in an induction motor, the actual fault frequency component is [16]:

$$f_{bre} = \left[\frac{k}{p} (1 - s) \pm s \right] f, \tag{1}$$

where k is the order of characteristic fault harmonic components; p is the number of poles, s is slip, and f is supply frequency. In Equation (1), the parameters of k and p are commonly chosen as $k/p = 1, 5, 7, 11, 13$, $k/p = 1$. When a broken rotor bar occurs, the fault characteristic component is $(1 \pm 2s) f$ and can be considered as an indication of the degree of rotor bar failure.

2.1.2. Analysis of Eccentricity Failure Mechanism

In practice, the air gap between the stator and rotor of an induction motor is essential, the difference between the static and dynamic eccentricity of the air gap is whether the minimum air gap position will change. Based on the stator current characteristics, the sideband components for frequencies of rotor air gap eccentricity fault can be determined as [4]:

$$f_{ec} = f_g \left[(R \pm n_d) \left(\frac{1 - s}{p} \right) \pm n_{ws} \right], \tag{2}$$

where R is the number of rotor bars, s is slip, f_{ec} is eccentricity frequency, f_g is electrical supply frequency, $n_d = \pm 1$, $n_{ws} = 1, 3, 5, 7, ...$, and p is pole-pairs defined in Equation (2). Therefore, electrical (current or instantaneous power) quantities can be analysed to identify eccentricity-related problems.

2.2. Signal Processing

2.2.1. Tunable Q-Factor Wavelet Transform

The wavelet transform and the short-time Fourier transform are both methods of analysis using the time-frequency domain, but the short-time Fourier transform has certain drawbacks. In the case of induction motor rotor faults, most of the signals collected are non-linear. The short-time Fourier transform is not ideal for processing such signals because of the difficulty in selecting the window function. The main difference between wavelet transform and short-time Fourier The main difference between the wavelet transform and the short-time Fourier transform is that the wavelet transform is not limited by the window function and provides a window that changes with frequency, adaptively following the different characteristics of the signal. The wavelet transform is not constrained by a window function and provides a window that changes with frequency, making it adaptive to the different characteristics of the signal and extracting valid information, making it very suitable for non-linear signal analysis.

In recent years, a new type of discrete wavelet transform, Tunable Q-factor Wavelet Transform (TQWT), has been proposed, which can pre-set the Q value and perfectly reconstruct the signal performance when analysing discrete signals. TQWT is superior to traditional wavelets in that it can adaptively adjust the Q value of the wavelet basis function by using the characteristics of the signal itself so that the signal can be better matched with the wavelet basis function. TQWT has three adjustable parameters, which are the quality factor Q, the oversampling rate r and the number of decomposition layers J. The expression of the quality Factor (Q) is given by Equation (3) as follows [17]:

$$Q = \frac{f_c}{B_w}, \tag{3}$$

where f_c is the centre frequency; B_w is the bandwidth.

The maximum number of decomposition layers J is determined by Q and r. The frequency response of the filter is also determined by Q and r. The Q factor affects the oscillatory characteristics of the wavelet waveform and an increase in the Q value increases the oscillation of the wavelet waveform, so setting the appropriate Q value directly

affects the accuracy of the TQWT. In the TQWT parameter setting, the quality factor Q value and the oversampling rate r are of vital importance, and in general, the r value is taken as 3, the Q value needs to be decided according to the signal characteristics, and the J value has no significant influence on signal decomposition.

2.2.2. Fractal Geometry

Traditional feature extraction methods make it difficult to accurately extract the nonlinear and nonsmooth features of fault signals, and the emergence of fractal geometry provides new ideas for such fault signals. Fractals can describe and portray anything in the world, which characterises the similarity between the whole and parts of an object, and the object under study is scale-independent. The fractal dimension is the unit of measure of a fractal and describes the roughness, irregularity, unevenness, and complexity of an object. Different types of fractal dimensions such as the box dimension, the information dimension, and the association dimension have been studied today.

In the field of signal processing, the box dimension is the simplest subdimension to compute the geometric scale of a signal and is widely used in various fields, both for self-similarity and non-self-similarity, and even for objects in higher dimensional spaces, and of the many fields, the field of self-similarity properties of signals is particularly prominent.

Principle of the box dimension: select several boxes whose sides are all of length x, and use the minimum number of boxes as possible to cover the object of study completely, and the number of its coverage is called $N(x)$, and then continuously reduce the length of the sides of the boxes, and repeat the above steps to obtain a series of points $(x, N(x))$, and fit these points by the least squares method and represent them in a logarithmic coordinate system, where the slope of the line obtained is the box dimension. The slope of the obtained line is the box dimension, which is defined as Equation (4) here [18]:

$$d_b = - \lim_{x \to \infty} \frac{logN(x)}{log(x)}. \tag{4}$$

2.3. Post-Processing and Diagnosis of Faults

2.3.1. Support Vector Machine

Support vector machines (SVMs) are widely used in fault diagnosis techniques, and many experts have applied them to the field of equipment fault multiclassification and made some achievements. It is suitable for analysing small samples of data and can maintain a high accuracy of multi-classification. In addition, it is not much affected by external abnormal factors and has good performance [19].

For input data x_i, where $i = 1, 2, 3, M$, with M = the total number of samples, assumed to belong to either of the two classes namely the 'positive' or 'negative' class. Let each of the classes associated with labels be $y_i = +1$ (positive class) and $y_i = -1$ (negative class), respectively. If the data is assumed to be linearly separable, it is possible to determine the hyperplane $f(x) = 0$ that separates the data between two classes [20]:

Regarding the input data x_i, (where $i = 1, 2, 3, ..., M$) and M denotes the total number of samples, it is believed that the samples fall into one of the two classes, the "positive" or "negative" class. Let $y_i = +1$ (positive class) and $y_i = -1$ (negative class) represent the corresponding classes linked with the labels. The hyperplane $f(x) = 0$ that divides the data into two classes may be found if it is assumed that the data is linearly separable [20]. It could be defined in Equation (5) as:

$$f(x) = w^T x + b = \sum_{j=1}^{M} w_j x_j + b = 0, \tag{5}$$

where w is a vector with M-dimensions and b is a scalar quantity. The position of the separating hyperplane is governed by a vector w and scalar b. The sign $[f(x)]$ is used to make a decision function for creating a hyperplane that classifies the input data to either of positive or negative class. Thus, discrete separating hyperplane should satisfy the constraints as Equation (6) [20]:

$$f(x_i) = +1, \qquad if \ y_i = +1 \tag{6}$$

$$f(x_i) = -1, \qquad if \ \ y_i = -1$$

Figure 4 shows a typical scenario of an ideal hyperplane for two data sets. Samples of data from two distinct classes are displayed below, with triangles denoting the negative class and squares the positive class. The ideal separating hyperplane is the one that creates the biggest margin—that is, the maximum distance—between the plane and the closest data. Support vectors are those data points that are closest to the hyperplane and are used to express the margin. The remaining feature set is eliminated following the support vector selection.
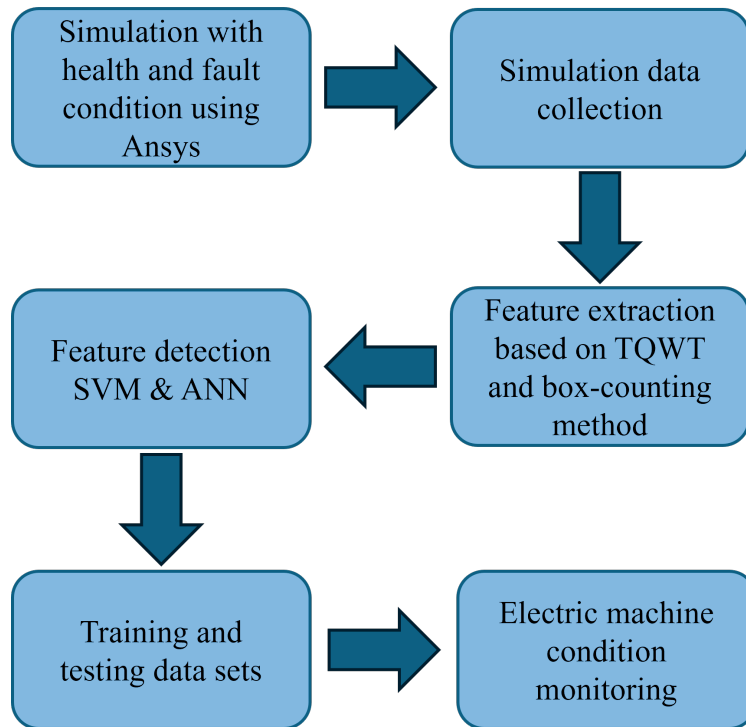
Figure 4. Hyperplane for classifying two classes with a maximum margin [21].

The process of SVM-based fault classification requires careful consideration while choosing a kernel function. The most widely used SVM kernel functions are Gaussian RBF, polynomial (quadratic, cubic), and linear; they are frequently used depending on the nature of the class separation [22]. Different nonlinear separation surfaces are produced by the various kinds of kernel functions. In this work, the SVM classifier with Gaussian RBF was utilized to classify the motor faults based on the retrieved and chosen features from the current signals.

2.3.2. Artificial Neural Network

To date, there are about 40 different neural network models. Depending on the type of connection, neural networks can be categorised into forward and feedback neural networks. A back propagation (BP) network is a multi-layer feed-forward neural network that gets its name from the fact that in network training, the adjustment of network weights in the training algorithm is the error backpropagation learning algorithm or BP learning algorithm [23]. Due to its simple structure, the number of adjustable parameters of the training algorithms and good manipulability, BP neural networks (BPNN) have gained wide practical applications [24]. One of the most significant aspects of the multi-layer perceptron structure is the selection of an optimal number of hidden layer neurons. The size of the hidden layer impacts the results significantly, and thus in this work, a hidden layer with 10 hidden nodes was used to compute classification accuracy. The relevant feature matrix obtained from reconstructed data was divided into three categories, i.e. 70% training data and 30% testing data to evaluate the performance of the neural network classifier.

Synapses (inputs and outputs), an adder unit, and an activation function with bias (b) as an external input make up a neuron. Each neuron's output, with the exception of input layer neurons, is calculated by multiplying the

input values x_i by their corresponding weights w_i. The resultant weighted value $w_i x_i$ is then coupled with a bias term (b) and runs via a transfer function f to get the neuron output o_j as displayed in Equation (7) [25].

$$o_j = f\left(\sum_{i=1}^{n} w_i x_i + b\right). \tag{7}$$

In a supervised learning method, the input (x_i) is presented to the network and a matching anticipated target (t_n) response is set at the output described in Equation (8) [25]:

$$\{x_1, t_1\}, \{x_2, t_2\}, \dots \{x_n, t_n\}, \tag{8}$$

where the neural network's input is denoted by x_n, and the matching target output is represented by t_n. Figure 5 depicts the conventional architecture of an ANN. Every neuron in the hidden layers is connected to all neurons in the layers above and below it in a weighted manner.
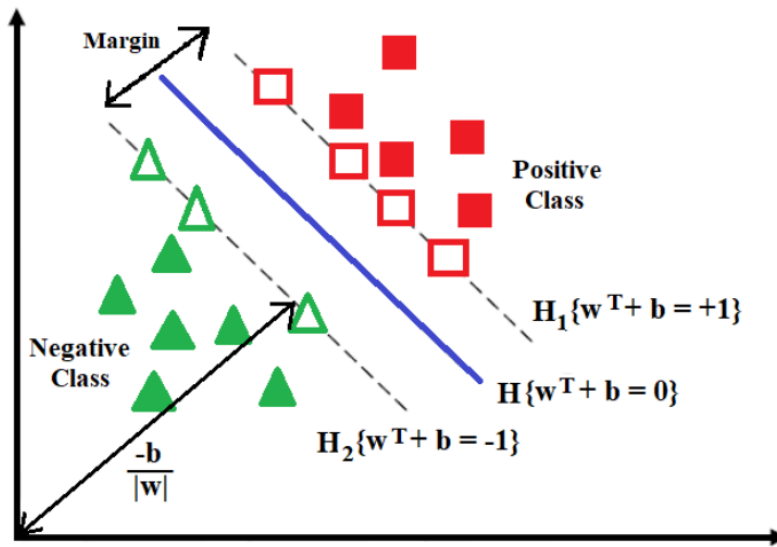

Figure 5. Artificial Neural Network [21].

3. Results and Discussion

In this section, two machine learning-based classifier algorithms—SVM and ANN—are used to classify four distinct operational scenarios.

3.1. Induction Motor Simulation Results

Based on theoretical analysis, the normal, broken bar, air gap static eccentricity and dynamic eccentricity of the induction motor are constructed with a limited element model, get the stator current signal data under the corresponding state, and carry out the spectrum analysis of the signal data to compare with the fault components calculated by the theoretical fault expression to verify the usability of the simulated signal data.

3.1.1. Analysis of Broken Rotor Bars Fault Model

In the finite element simulation, the squirrel cage is made of aluminium and the motor is modelled for both normal and broken rotor conditions by changing the electrical conductivity parameter, as shown in Table 2. Under normal conditions, the conductivity parameter is set to 38,000,000 and the relative permeability parameter to 1, as shown in Table 2a; when the motor has a broken rotor, the conductivity parameter is changed to 2 and the relative permeability parameter remains unchanged, as shown in Table 2b. The finite element model of the induction motor rotor with broken bars is shown in Figure 6.

Table 2. Material parameters setting: (**a**) Healthy condition, and (**b**) Faulty condition with 4 broken rotor bars.

(a)				(b)		
Properties of the Material				Properties of the Material		
Name	Type	Value	Units	Name	Type	Value
Relative Permeability	Simple	1.000021		Relative Permeability	Simple	1.00021
Bulk Conductivity	Simple	38,000,000	Siemens/m	Bulk Conductivity	Simple	2
Magnetic Coercivity	Vector			Magnetic Coercivity	Vector	
Magnitude	Vector Mag	0	A/m	Magnitude	Vector Mag	0
Core Loss Model		None	w/m^3	Core Loss Model		None
Mass Density	Simple	2689	Kg/m^3	Mass Density	Simple	2689
Composition		Solid		Composition		Solid

(a) Healthy condition
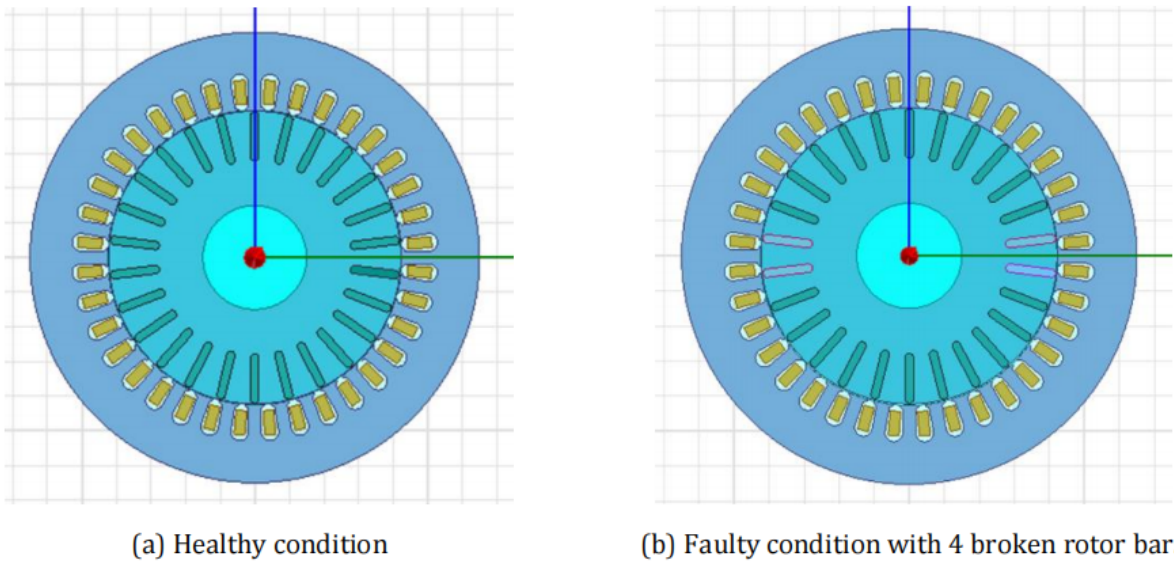
(b) Faulty condition with 4 broken rotor bars

Figure 6. 2D finite element model of the motor with BRB fault.

The stator current waveforms of the induction motor in normal condition and with a broken bar fault are shown in Figure 7. The stator current curve of the normal motor is sinusoidal with time, while the stator current of the fault with broken bars is unbalanced and the waveform is seriously distorted. Spectral analysis of the simulated stator current waveform shows the results in Figure 8. The spectrum shows significant side frequencies on both sides of the 50 Hz main frequency, with side frequencies at 47.5 Hz and 52.5 Hz, indicating that a fault characteristic frequency of $(1\pm2s)f$ exists in the stator current when the motor has a broken bar, which verifies the accuracy of the mechanics.

In the actual operation process, induction motor rotor broke bar fault monitoring and fault diagnosis is particularly important, but the fault frequency component is not easy to find or even confused with other fault components, there are three main reasons: First, the rotor bar is broken at the initial stage, the fault characteristics information is not obvious, the fault frequency component is submerged in the fundamental signal. Second, the small rate of rotation difference will also cause the broken bar fault frequency to be extremely weak. Third, when the induction motor is in normal operation, the collected stator current signal may also contain the $(1\pm2s)f$ fault component. All these factors can lead to misdiagnosis and affect the reliability and accuracy of fault monitoring. In summary, it

is of great importance to obtain the actual stator current data for the diagnosis of broken rotor bars in induction motors.
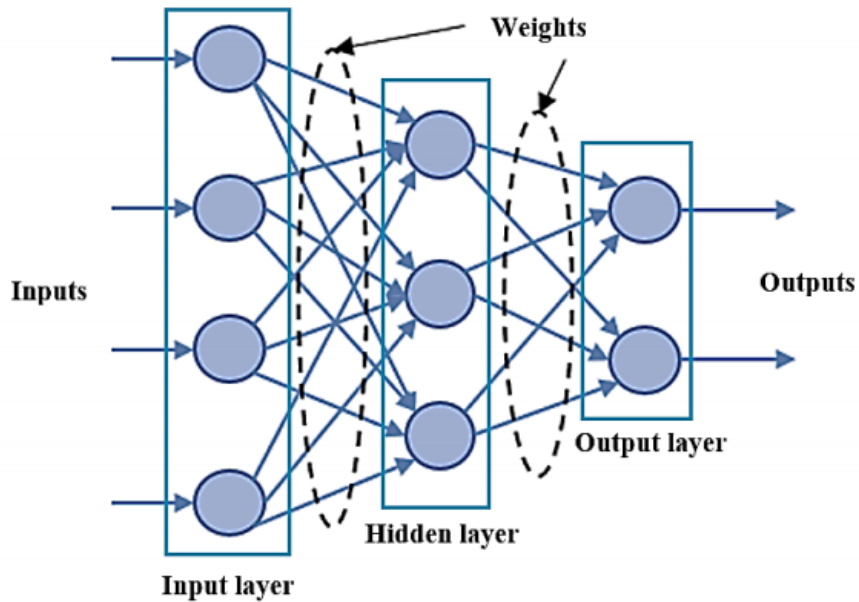

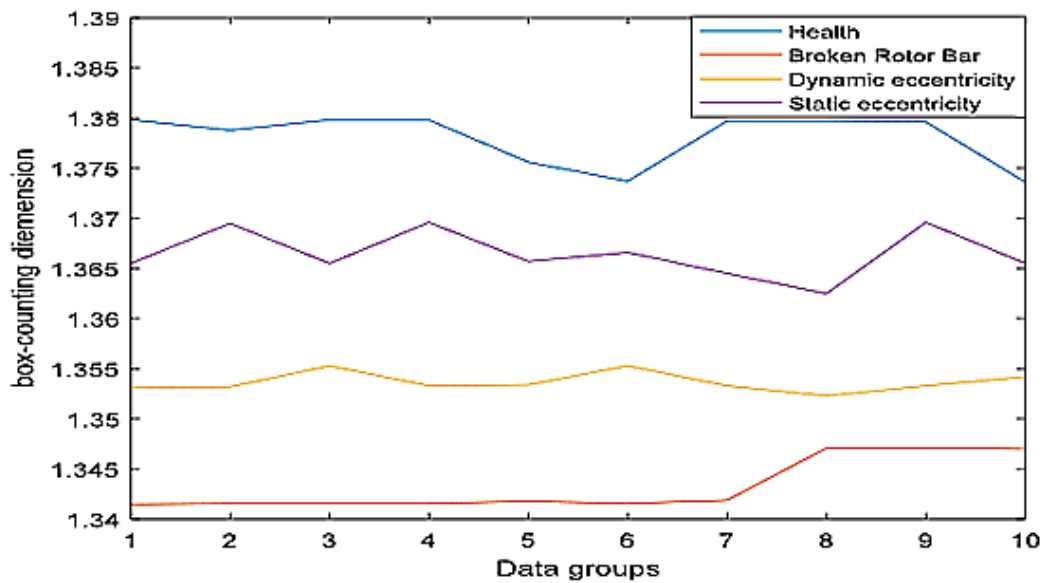**Figure 7.** Time domain waveforms of current signals with BRB fault.

Figure 8. Frequency domain waveforms of current signals with BRB fault.

3.1.2. Analysis of Eccentricity Fault Model

To further obtain the magnetic field distribution and stator current variation of the induction motor under an air gap eccentricity fault, a simulation model of the induction motor under different eccentricity faults needs to be established. Following the simulation method described in the previous section, a finite element model of a normal induction motor is first created in Maxwell, based on which the eccentricity fault is set up [26].

The normal air gap length of the induction motor model was 0.5 mm. The parameters of the motor model in

its normal state were modified so that the rotor part was offset from the bearing by different degrees (i.e. different degrees of eccentricity), thus creating an air gap eccentricity fault with different degrees of eccentricity, and the motor model is shown in Figure 9.
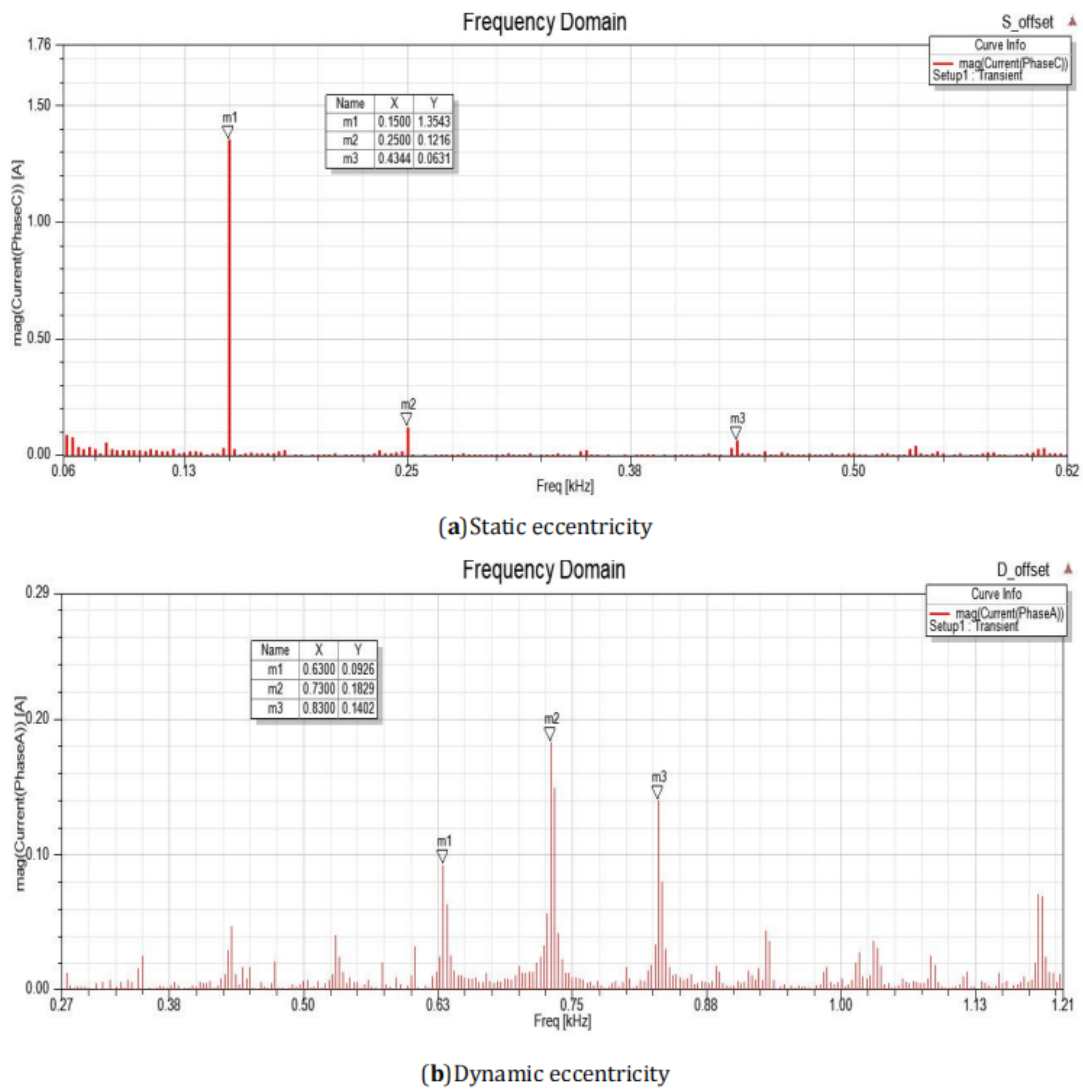

(a) Static eccentricity

(b) Dynamic eccentricity

Figure 9. 2D finite element model of the motor with eccentricity fault.

After the simulation, the time domain waveform of the stator current was obtained, as shown in Figure 10. The time domain waveforms of the stator current signals are analysed separately for normal, static and dynamic eccentricity conditions. The stator current under an air gap eccentricity fault appears unbalanced, with small distortions in the waveform and the difference between static and dynamic eccentricity is not significant. The harmonic components generated when the air gap is eccentric cannot be visualised from the figure. Therefore, a spectral analysis of the stator current signal was carried out to further investigate the fault components generated during the fault.

According to the design parameters of the simulated motor model, the characteristic frequencies of static eccentricity fault in the stator current are 165.9 Hz, 265.9 Hz and 465.9 Hz, which are calculated according to Equation (2). and the spectral analysis of the simulated stator current shows 150 Hz, 250 Hz, 434.4 Hz in Figure 11a. The characteristic frequencies of dynamic eccentricity fault in the stator current are 602.35 Hz, 702.35 Hz and 802.35 Hz, simulation results show 630 Hz, 730 Hz and 830 Hz in Figure 11b. The results obtained from the simulation deviate a little from the theoretical results and the data are reasonable.
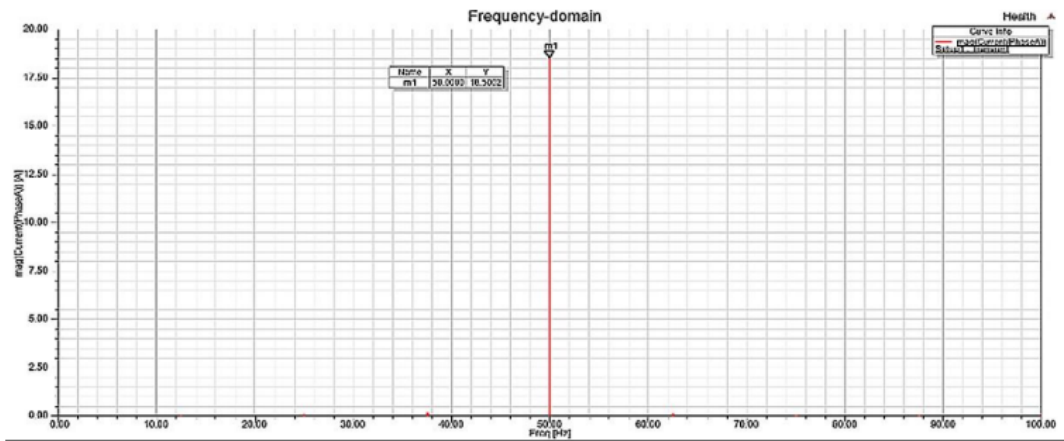
(a) Healthy condition
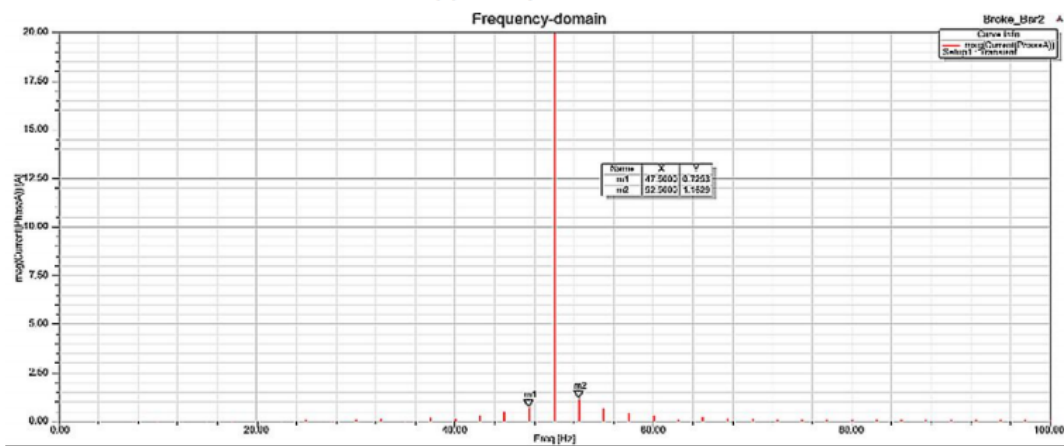
(b) Faulty condition with 4 broken rotor bars

Figure 10. Time domain waveforms of current signals with eccentricity fault.

Similar to the case of broken rotor bar faults in induction motors, in actual operation, the frequency of the current side frequency is extremely small and not easy to detect in the early stage of the air gap eccentricity fault. At the same time, the frequency component of the air gap eccentricity is similar to the side frequency band at the beginning of the broken rotor bar fault which makes it easy to misjudge a broken bar fault as an air gap eccentricity fault and affects the reliability of the fault detection. Therefore, it is of great importance to obtain the stator current from the actual situation for the diagnosis of air gap eccentricity faults in motors.
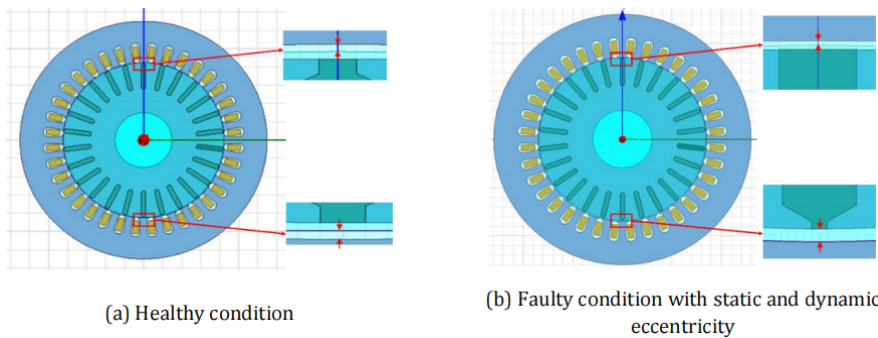

(a) Healthy condition

(b) Faulty condition with static and dynamic eccentricity

Figure 11. Frequency domain waveforms of current signals with eccentricity fault.

3.2. Feature Extraction

3.2.1. Based on the Box-Counting Method

The box-counting dimension is calculated for the stator current signals in four cases: normal, broken bar, static air gap eccentricity and dynamic air gap eccentricity, and it can be seen from Figure 12: the box-counting dimension in the four cases is not obvious, especially the box dimension in the case of dynamic eccentricity and static eccentricity are too close to each other, which is not able to differentiate the type of faults effectively so that the box dimension algorithm is not very effective for the induction motor rotor fault feature extraction.
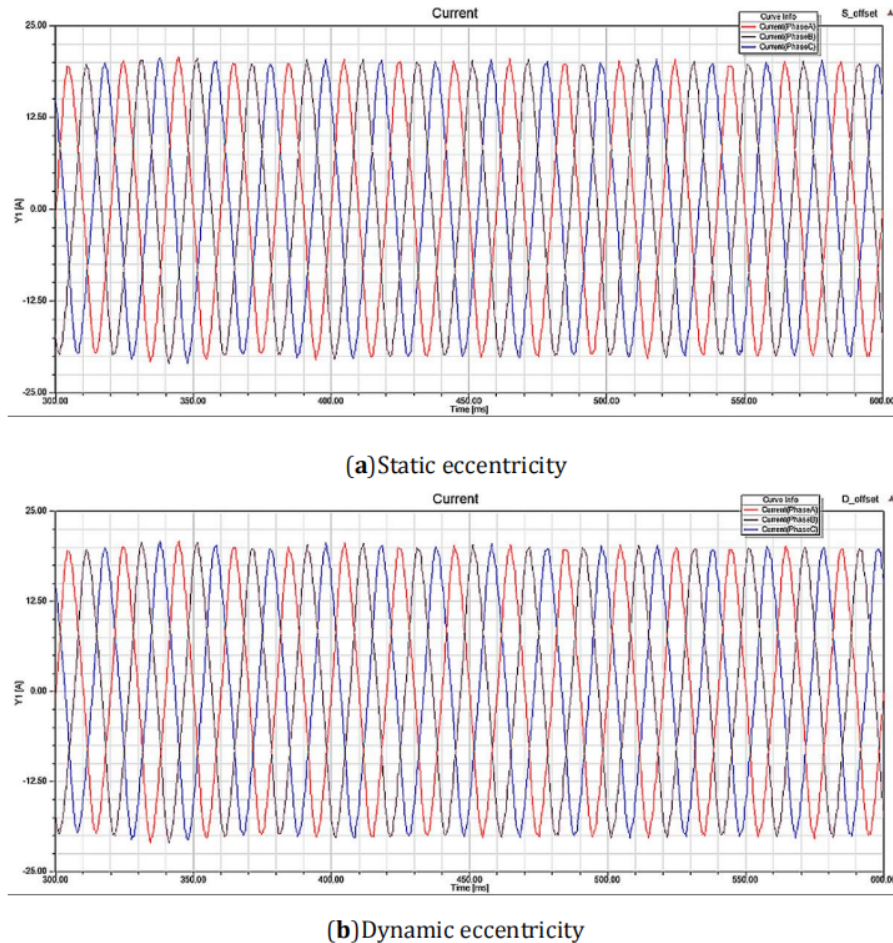

(a)Static eccentricity

(b)Dynamic eccentricity

Figure 12. Box-counting dimensions of current signals.

3.2.2. Tunable Q-Factor Wavelet Transform (TQWT)-Based and Box-Counting Metho

When TQWT is selected for stator current signal feature extraction, there are meaningless subband components (such as harmonics generated in the signal) in the subbands obtained by decomposition. Therefore, these meaningless components should be eliminated, and the signal could be reconstructed from the remaining subband components so that the reconstructed signal has a relatively large number of fault components. The fault component has a relatively large energy, and it is easy to obtain the fault component, after which the calculation of the number of subdimensions is carried out, which is very effective for distinguishing different faults. Figure 13 shows the distribution of current signal energy using TQWT in four different cases.

The Tunable Q Wavelet Transform is fully discrete and works well to localise and analyse signals. For signal processing algorithms, the transform maintains the energy property (Parseval's theorem), i.e., the total energy of the wavelet coefficients is equal to the total energy of the signal. As a result, this study selects the subbands that

contain more fault information through the subband energy values, as can be seen in Figure 13: the energy ratio of different fault subbands is different, and the subbands with larger energy values are subbands 7, 8, and 9 for the four motor cases of normal, broken bars, static air-gap eccentricity, and dynamic air-gap eccentricity; therefore, the three subbands are extracted and reconstructed to obtain the new signal, as shown in Figure 14.
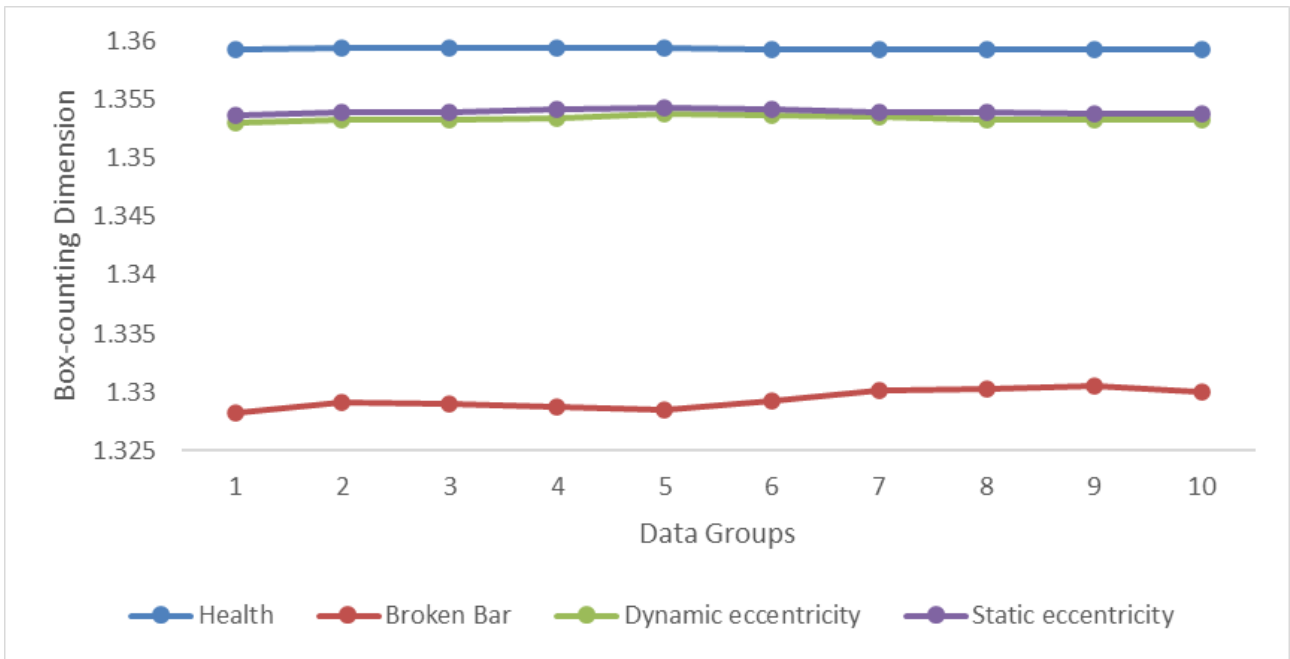

Figure 13. Distribution of current subband signal energy in TQWT.

(a) Health

(b) Broken rotor bars

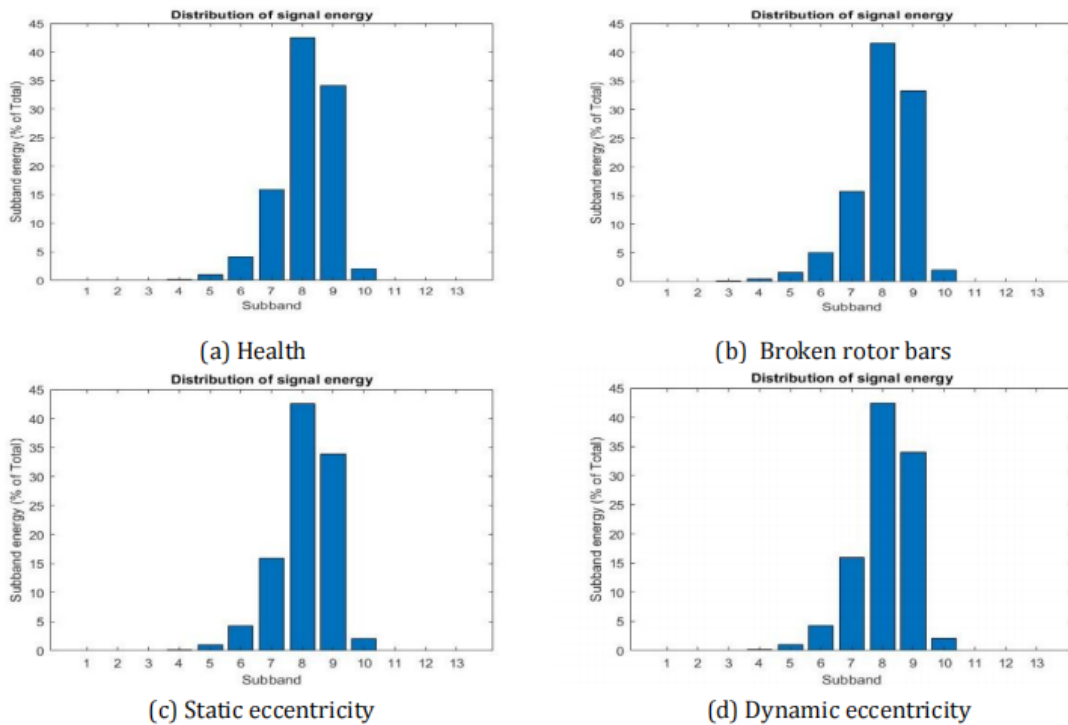(c) Static eccentricity

(d) Dynamic eccentricity

Figure 14. Reconstruction current signals in four situations.

The simplest box-counting method is chosen to divide the reconstructed signals into dimensions, and the box-counting dimension values obtained are used to distinguish the normal, broken bars, static eccentricity and dynamic eccentricity in the four operating conditions. As shown in Figure 15 the line graph of the box-counting dimension for normal, broken bars, static eccentricity and dynamic eccentricity. The box-counting dimension of each reconstructed current signal of the induction motor is shown in Table 3.
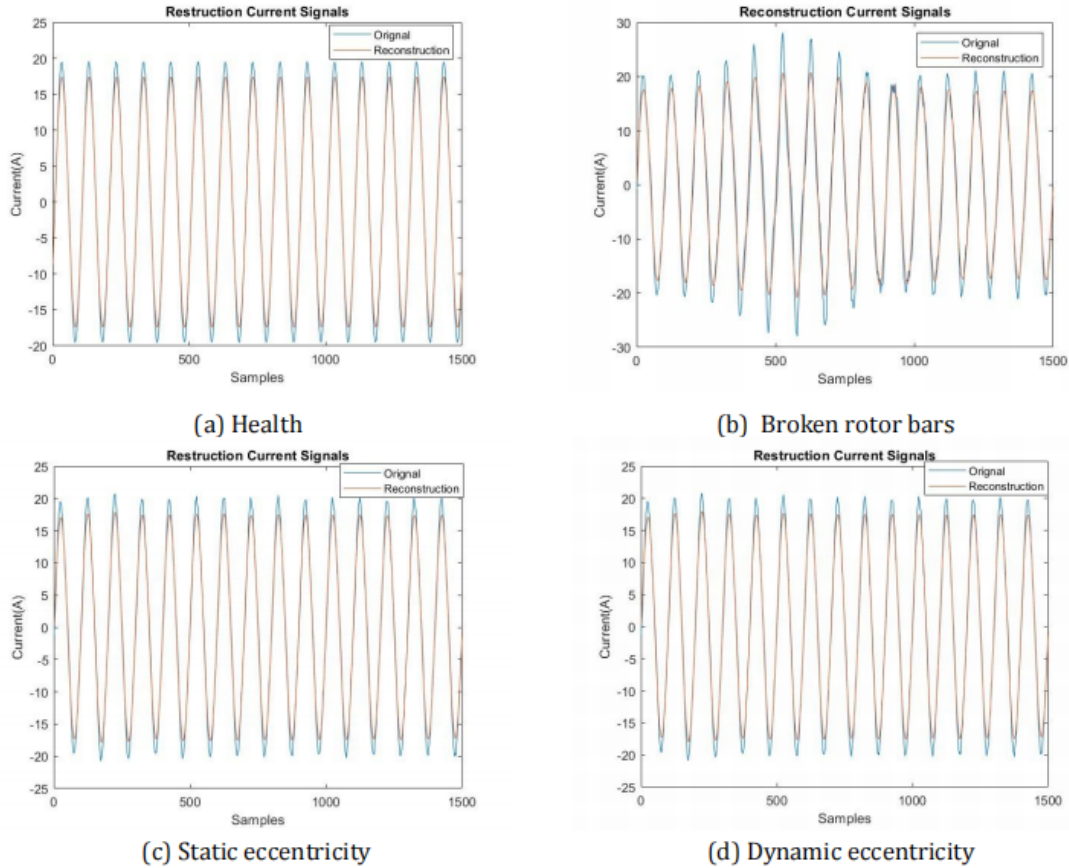
(a) Health

(b) Broken rotor bars

(c) Static eccentricity

(d) Dynamic eccentricity

Figure 15. Box-counting dimensions of TQWT reconstructed signals.

Table 3. Box-counting dimension of each reconstructed signal.

No.	Health	Broken Bar	Dynamic Eccentricity	Static Eccentricity
1	1.3798	1.3415	1.3531	1.3655
2	1.3788	1.3416	1.3532	1.3695
3	1.3798	1.3416	1.3553	1.3655
4	1.3798	1.3416	1.3533	1.3696
5	1.3756	1.3418	1.3534	1.3657
6	1.3737	1.3416	1.3553	1.3666
7	1.3797	1.3419	1.3533	1.3645
8	1.3797	1.3471	1.3523	1.3625
9	1.3796	1.3471	1.3533	1.3696
10	1.3736	1.347	1.3542	1.3655

From Figure 15, the four cases of faults can be distinguished clearly, so the combined algorithm of TQWT and box-counting dimension can be an effective method in the feature extraction method of induction motor faults, and

can also be used as a feature set for classification and identification in the next step of fault diagnosis.

3.3. Feature Classification

Artificial Intelligence is widely used in fault diagnostic techniques, and many experts have applied it to the field of equipment fault multiclassification and have made achievements. In this section, the results of SVM and ANN for small sample data analysis will be discussed.

3.3.1. Classifier Used Support Vector Machine

The support vector machine algorithm is mainly for the binary classification problem, and the standard support vector machine can only classify the data samples into positive class samples and negative class samples. While there are multiple fault types in induction motor rotor faults, so when using the SVM classification algorithm to solve the classification problem, it is necessary to implement the multi-classification function.

The fault feature samples are extracted by the feature extraction method adopted in this work, and the obtained feature sample data are used as input data for subsequent fault diagnosis. When the feature sample data are classified and identified by the SVM classifier, the sample data are firstly divided into two parts according to a certain ratio: the training set and the test set, which are also normalised.

From the simulation results, 10 groups of health, broken bar, air gap static eccentricity and dynamic eccentricity stator current signal data are extracted, each group has 1500 points, and a total of 40 groups constitute the fault feature samples, from which 7 groups each with a total of 28 groups are selected as the training set to train the SVM classifier, and the remaining 12 groups are used as the test set to carry out the fault diagnostic study to find the optimal fault diagnostic model.

As the input of faults, the dimensional numbers of feature sets are used to represent four induction motor rotor operating conditions, namely normal, broken bars, static eccentricity and dynamic eccentricity, with categories 1, 2, 3 and 4, respectively. The most common Gaussian radial basis function kernel (RBF kernel) function and parameter auto-optimisation methods are chosen to record the classification recognition rate of the fault test set samples, the diagnostic results obtained are shown in Figure 16.
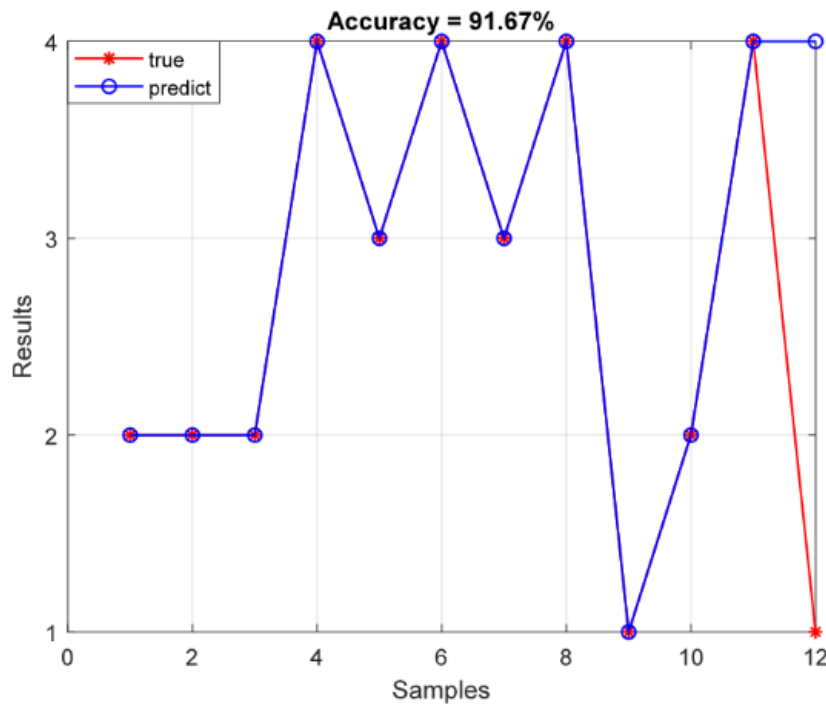

Figure 16. SVM model test results: The vertical axis shows numbers 1 to 4 which are related to normal, broken bars, static eccentricity, and dynamic eccentricity.

The category labels 1, 2, 3 and 4 in Figure 16 represent four kinds of induction motor operating conditions, namely, healthy, rotor broken bar, air gap static eccentricity and dynamic eccentricity, and the test sample set are 3 groups each with a total of 12 groups, and the diagnosis results of the SVM classifier are shown in Table 4.

Table 4. SVM diagnostic result.

No.	Health	Broken Bar	Dynamic Eccentricity	Static Eccentricity	Total
Samples	4	4	4	4	12
Misjudgments	1	0	0	0	1
Accuracy	75%	100%	100%	100%	91.67%

From Table 3, it can be seen that the induction motor rotor healthy case and the air gap dynamic eccentricity case are more likely to be confused with each other, while the number of misclassifications in the case of rotor broken bars and the air gap static eccentricity case is smaller, resulting in an overall recognition rate of 91.67%. Due to the small dataset of this project, the training results are not fully adequate, and the SVM classifier can be optimised by increasing the dataset in the future.

3.3.2. Classifier Used Back Propagation Neural Network

The number of neurons in the input layer is 1, which represents 1 feature vector we selected; the number of neurons in the intermediate layer is taken as 10; and the output layer is 4, which represents the four conditions of normal, rotor broken bar, static eccentricity and dynamic eccentricity. The transfer function of neurons in the hidden layer is logsig with S-type logarithmic function, meanwhile, the transfer function of neurons in the output layer is also logsig with S-type logarithmic function, and the training function is selected as traindx with gradient descent adaptive learning rate. The number of times of training is set to 500, the training target is 0.001, and the learning rate is 0.01. The same samples as SVM classifiers are selected for training, and the following test results are shown in Figure 17.
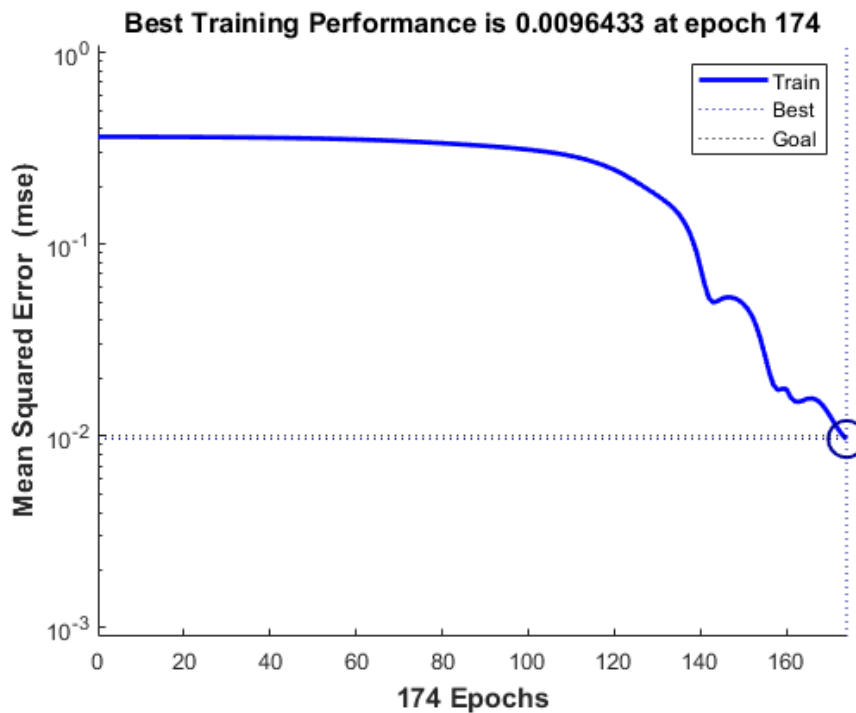

Figure 17. Training set performance of ANN.

It is known from the vertical coordinate of Figure 17, which measures the performance of the network by the mean square error. From the figure, it can be seen that as the number of iterations increases, the mean square error gets smaller and the performance is better, and after 174 training sessions, the network converges.

The actual output of the validation samples obtained is compared with the target output as shown in Table 5. In Table 4, $(y_1, y_2, y_3, y_4) = (1,0,0,0)$, representing the normal state; $(y_1, y_2, y_3, y_4) = (0,1,0,0)$, representing the broken rotor bar state; $(y_1, y_2, y_3, y_4) = (0,0,1,0)$, representing the static eccentricity state; $(y_1, y_2, y_3, y_4) = (0,0,0,1)$, representing the dynamic eccentricity state. Based on the comparison between the actual output matrix of the validation samples calculated above and the corresponding target matrix, the correct rate of the validation samples is calculated. For 12 test samples, the number of correct samples is 12, so the correctness rate of the test samples can be obtained as follows 100%.

Table 5. ANN test result.

No.	Actual Output	Targeted Output	Accuracy
1	(0,1,0,0)	(0,1,0,0)	Correct
2	(0,1,0,0)	(0,1,0,0)	Correct
3	(0,1,0,0)	(0,1,0,0)	Correct
4	(0,0,0,1)	(0,0,0,1)	Correct
5	(0,0,1,0)	(0,0,1,0)	Correct
6	(0,0,0,1)	(0,0,0,1)	Correct
7	(0,0,1,0)	(0,0,1,0)	Correct
8	(0,0,0,1)	(0,0,0,1)	Correct
9	(1,0,0,0)	(1,0,0,0)	Correct
10	(0,1,0,0)	(0,1,0,0)	Correct
11	(0,0,0,1)	(0,0,0,1)	Correct
12	(1,0,0,0)	(1,0,0,0)	Correct

4. Conclusions

In this paper, we are exploring how to diagnose motor issues through the analysis of motor current signals by utilizing Support Vector Machine (SVM) and Block Perceptron Neural Network (BPNN) classification techniques. The data we used for this analysis was gathered from a simulation by ANSYS Maxwell. This data was then divided into distinct, non-overlapping segments. After that, we extracted and normalized the relevant features. To simplify the processing and enhance the classification accuracy, we used techniques like TQWT and determining the size of the current boundary boxes. It was found that the classification performance of the BPNN technique in identifying motor faults was superior to that of SVM. The highest classification rate was reached with an Artificial Neural Network (ANN) trained using the traindx function, achieving a classification accuracy of 100%, which was 8.33% higher than what SVM could achieve. The strategy of selecting features using TQWT and box dimensions was found to be successful in decreasing the data size while increasing the accuracy of the classification. While both approaches to identifying motor faults provided good results, the BPNN technique emerged as the better choice and could be effectively applied to similar tasks in fault detection and classification. The positive outcomes from this study highlight the effectiveness of this method in creating reliable and precise fault diagnosis techniques.

Although the method of this thesis has achieved some results, due to the actual working conditions, people's requirements for rotor fault diagnosis continue to improve, and this research method is still insufficient. At present, the rotor air gap eccentricity faults of induction motors produce large additional components, this thesis does not preprocess the original signal, and further in-depth research is needed to study the reasons for the large additional components and their processing methods. In the feature extraction method, the complexity of the tunable Q wavelet algorithm is higher, due to the limited research time, the parameter setting of the tunable Q wavelet algorithm is only superficial knowledge, and further in-depth research is needed. In this study of fault feature extraction methods, a single feature quantity is used, although the extraction of feature vectors is effective, multiple feature quantities may be a more comprehensive portrayal of fault characteristics, and the subsequent fault diagnosis and identification more accurate. Therefore, the redundant data of the fault feature volume can be eliminated by using

the feature fusion method to extract the core content of the fault in the subsequent research.

5. Future Works

It is expected that the proposed strategy will be implemented in wireless sensor networks due to its small size and lightweight, which can be used for condition monitoring and fault diagnosis of motors installed in remote areas. The research work could also consider the use of more suitable fault indicators and different types of advanced classification algorithms.

Deep Learning has shown great potential in motor fault detection and classification. CNNs can effectively extract features from complex sensor data, such as vibration signals, to identify patterns indicative of faults. By classifying these patterns, CNNs can accurately predict the type and severity of a fault. Additionally, RNNs can be employed for time-series analysis, allowing them to detect anomalies and predict faults based on historical data trends. Ensemble methods like boosting and bagging can also be applied to improve classification accuracy and robustness by combining multiple models' predictions. Hybrid models that combine different machine-learning approaches provide further enhancements in fault detection and prediction. Moreover, the implementation of IoT technology in industrial settings offers numerous benefits, including improved efficiency and reduced downtime. By integrating smart sensors into industrial equipment, real-time data collection and monitoring become possible, enabling predictive maintenance and reducing the likelihood of costly repairs down the line. In addition, edge computing can help reduce latency in data transmission by processing data closer to the source, leading to faster response times and more effective fault detection. These advancements have the potential to transform industrial operations, making them more efficient, productive, and profitable than ever before.

Institutional Review Board Statement

Not applicable.

Informed Consent Statement

Not applicable.

Data Availability Statement

Not applicable.

Conflicts of Interest

The authors declare no conflict of interest.

References

1. Konar, P.; Chattopadhyay, P. Bearing fault detection of induction motor using wavelet and Support Vector Machines (SVMs). *Appl. Soft Comput.* **2011**, *11*, 4203–4211. [CrossRef]
2. Gangsar, P.; Tiwari, R. Signal based condition monitoring techniques for fault detection and diagnosis of induction motors: A state-of-the-art review. *Mech. Syst. Signal Process.* **2020**, *144*, 106908. [CrossRef]
3. O'Donnell, P.; Heising, C.; Singh, C.; Wells, S. Report of large motor reliability survey of industrial and commercial installations. iii. *IEEE Trans. Ind. Appl.* **1987**, *23*, 153–158.
4. Choudhary, A.; Goyal, D.; Shimi, S.L.; Akula, A. Condition Monitoring and Fault Diagnosis of Induction Motors: A Review. *Arch. Comput. Methods Eng.* **2019**, *26*, 1221–1238. [CrossRef]
5. Siddique, A.; Yadava, G.; Singh, B. A Review of Stator Fault Monitoring Techniques of Induction Motors. *IEEE Trans. Energy Convers.* **2005**, *20*, 106–114. [CrossRef]
6. Sarma, N.; Melecio, J.; Mohammed, A.; Djurovic, S.; Tshiloz, K. An experimental study of winding fault induced slot harmonic effects in the cage rotor induction machine stator current. In Proceedings of the 8th IET International Conference on Power Electronics, Machines and Drives (PEMD 2016), Glasgow, UK, 19–21 April 2016.
7. Pillay, P.; Xu, Z. Motor current signature analysis. In Proceedings of the IAS'96. Conference Record of the 1996 IEEE Industry Applications Conference Thirty-First IAS Annual Meeting, San Diego, CA, USA,6–10 October 1996; IEEE: Piscataway, NJ, USA, 1996; Volume 1, pp. 587–594.
8. Granda, D.; Aguilar, W.G.; Arcos-Aviles, D.; Sotomayor, D. Broken Bar Diagnosis for Squirrel Cage Induction Motors Using Frequency Analysis Based on MCSA and Continuous Wavelet Transform. *Math. Comput. Appl.* **2017**, *22*, 30. [CrossRef]
9. Vanraj; Goyal, D.; Saini, A.; Dhami, S.S.; Pabla, B.S. Intelligent predictive maintenance of dynamic systems using condition monitoring and signal processing techniques—A review. In Proceedings of the 2016 International Conference on Advances in Computing, Communication, & Automation (ICACCA) (Spring), Dehradun, India, 8–9 April 2016; pp. 1–6.
10. Kudelina, K.; Vaimann, T.; Asad, B.; Rassolkin, A.; Kallaste, A.; Demidova, G. Trends and challenges in intelligent condition monitoring of electrical machines using machine learning. *Appl. Sci.* **2021**, *11*, 2761. [CrossRef]
11. Tian, Z. An artificial neural network method for remaining useful life prediction of equipment subject to condition monitoring. *J. Intell. Manuf.* **2009**, *23*, 227–237. [CrossRef]
12. Deng, Y.; Ren, Z.; Kong, Y.; Bao, F.; Dai, Q. A Hierarchical Fused Fuzzy Deep Neural Network for Data Classification. *IEEE Trans. Fuzzy Syst.* **2016**, *25*, 1006–1012. [CrossRef]
13. Awad, M.; Khanna, R. Support vector machines for classification. In *Efficient Learning Machines: Theories, Concepts, and Applications for Engineers and System Designers*; Apress: Berkeley, CA, USA, 2015; pp. 39–66.
14. Widodo, A.; Yang, B.-S. Wavelet support vector machine for induction machine fault diagnosis based on transient current signal. *Expert Syst. Appl.* **2007**, *35*, 307–316. [CrossRef]
15. Ferkova, Z. Comparison of two-phase induction motor modeling in ANSYS Maxwell 2D and 3D program. In Proceedings of the 2014 ELEKTRO, Rajecke Teplice, Slovakia, 19–20 May 2014; pp. 279–284.
16. Basak, D.; Tiwari, A.; Das, S.P. Fault diagnosis and condition monitoring of electrical machines—A Review. In Proceedings of the 2006 IEEE International Conference on Industrial Technology, Mumbai, India, 15–17 December 2006; pp. 3061–3066.
17. Kong, Y.; Wang, T.; Chu, F. Adaptive TQWT filter based feature extraction method and its application to detection of repetitive transients. *Sci. China Technol. Sci.* **2018**, *61*, 1556–1574. [CrossRef]
18. Liebovitch, L.S.; Toth, T. A fast algorithm to determine fractal dimensions by box counting. *Phys. Lett. A* **1989**, *141*, 386–390. [CrossRef]
19. Baccarini, L.M.R.; Silva, V.V.R.; Menezes, B.R.; Caminhas, W.M. SVM practical industrial application for mechanical faults diagnostic. *Expert Syst. Appl.* **2011**, *38*, 6980–6984. [CrossRef]
20. Pöyhönen, S. *Support Vector Machine Based Classification in Condition Monitoring of Induction Motors*; Helsinki University of Technology: Espoo, Finland, 2004.
21. Sharma, A.; Mathew, L.; Chatterji, S.; Goyal, D. Artificial Intelligence-Based Fault Diagnosis for Condition Monitoring of Electric Motors. *Int. J. Pattern Recognit. Artif. Intell.* **2020**, *34*, 2059043. [CrossRef]
22. Yin, Z.; Hou, J. Recent advances on SVM based fault diagnosis and process monitoring in complicated industrial processes. *Neurocomputing* **2016**, *174*, 643–650. [CrossRef]
23. Yang, B.-S.; Han, T.; Yin, Z.-J. Fault diagnosis system of induction motors using feature extraction, feature selection and classification algorithm. *JSME Int. J. Ser. C Mech. Sys. Mach. Elem. Manuf.* **2006**, *49*, 734–741.
24. Long, Z.; Zhang, X.; Zhang, L.; Qin, G.; Huang, S.; Song, D.; Shao, H.; Wu, G. Motor fault diagnosis using attention

mechanism and improved adaboost driven by multi-sensor information. *Measurement* **2020**, *170*, 108718.

25. Tyagi, C.S. A comparative study of SVM classifiers and artificial neural networks application for rolling element bearing fault diagnosis using wavelet transform preprocessing. *Int. J. Mech. Mechatron. Eng.* **2008**, *2*, 904–912.

26. Honarvar Shakibaei Asli, B. Analysis and simulations of eccentric rotors of rotating machinery in polar space. *World Appl. Sci. J.* **2012**, *17*, 1675–1682.

Publisher's Note: The views, opinions, and information presented in all publications are the sole responsibility of the respective authors and contributors, and do not necessarily reflect the views of UK Scientific Publishing Limited and/or its editors. UK Scientific Publishing Limited and/or its editors hereby disclaim any liability for any harm or damage to individuals or property arising from the implementation of ideas, methods, instructions, or products mentioned in the content.